Supplementary Information for "Penetrant shape effects on activated dynamics and selectivity in polymer melts and networks based on self-consistent cooperative hopping theory"

Baicheng Mei [a,d] and Kenneth S. Schweizer [*a,b ,c,d]

[a.] *Department of Materials Science, University of Illinois, Urbana, IL 61801, USA*

[b.] *Department of Chemistry, University of Illinois, Urbana, IL 61801, USA*

[c.] *Department of Chemical and Biomolecular Engineering, University of Illinois, Urbana, IL 61801, USA*

[d.] *Materials Research Laboratory, University of Illinois, Urbana, IL 61801, USA*

[*] kschweiz@illinois.edu

Three topics are addressed here: (i) some additional technical background concerning the well-known Polymer Reference Interaction Site Model (PRISM) theory of structure [1-5], (ii) some additional technical background for the Elastically Collective Nonlinear Langevin Equation (ECNLE) [1, 3, 6, 7] and Self-Consistent Cooperative Hopping (SCCH) [2, 8-10] dynamical theories, and (iii) additional calculations and results that support the discussions in the main text.

I. PRISM Theory for Structural Correlations

A. Polymer model and structural correlations

Under the site equivalency simplification for homopolymers, PRISM theory [1-5] consists of a single scalar integral equation which in Fourier transform space is given by [1-5]

$$h_{\mathrm{mm}}(q) = \omega_{\mathrm{m}}(q)C_{\mathrm{mm}}(q)\omega_{\mathrm{m}}(q) + \rho\omega_{\mathrm{m}}(q)C_{\mathrm{mm}}(q)h_{\mathrm{mm}}(q) = \omega_{\mathrm{m}}(q)C_{\mathrm{mm}}(q)S_{\mathrm{mm}}(q) \quad (1)$$

Here $h_{\mathrm{mm}}(q)$ is the Fourier transform of the intermolecular site-site total correlation function $h_{\mathrm{mm}}(r) = g_{\mathrm{mm}}(r) - 1$ with $g_{\mathrm{mm}}(r)$ the radial distribution or pair correlation function, $C_{\mathrm{mm}}(r)$

is the intermolecular site-site direct correlation function, and $S_{\mathrm{mm}}(q)$ is the collective or static structure factor. Using Eq.(1) in conjunction with the Percus-Yevick (PY) closure [4, 5, 8, 11, 12] and a polymer model (the semi-flexible chain (SFC) model is adopted [13, 14]) for the intramolecular structure factor $\omega_{\mathrm{m}}(q)$, the intermolecular site-site pair correlation functions can be computed numerically.

Because we focus on the dynamics of a Kuhn segment instead of a single interaction site of the SFC model, the relationship between the structural correlation functions of a Kuhn segment (denoted by subscript "K") and a site (also called matrix, denoted by a subscript "m") is required. Since the Kuhn segment is treated as a dynamically rigid particle at a center-of-mass (CM) level, the relationship is [15-18]

$$S_{\mathrm{KK}}(q) = S_{\mathrm{mm}}(q)/\omega_{\mathrm{K}}(q), C_{\mathrm{KK}}(q) = N_{\mathrm{K}}\omega_{\mathrm{K}}(q)C_{\mathrm{mm}}(q) \quad (2)$$

Eq.(2) is not relevant to PRISM theory calculations at the interaction site level, but does enter the dynamical theories formulated at the Kuhn scale (see section II). The intramolecular structure factor at the Kuhn segment level, ω_{K}, is given in the literature [2]; as discussed previously, setting $\omega_{\mathrm{K}} = 1$ or $\omega_{\mathrm{K}} = \omega_{\mathrm{m}}$ in the dynamic theories has minor influence on the predicted results [2].

B. Molecular penetrant models and packing correlations.

PRISM theory relates $S_{\mathrm{mm}}(q)$ and $h_{\mathrm{mp}}(q)$ as

$$h_{\mathrm{mp}}(q) = \omega_{\mathrm{p}}(q)C_{\mathrm{mp}}(q)S_{\mathrm{mm}}(q) \quad (3)$$

where $C_{\mathrm{mp}}(q)$ is the Fourier transform of the penetrant-polymer site-site direct correlation function and $\omega_{\mathrm{p}}(q)$ is the penetrant intramolecular structure factor that is easily computed from the geometry of rigid molecules. Eq.(3) is closed using the PY approximation.

II. Background for Dynamic Theories

A. ECNLE theory for pure polymer melts and networks

The foundational starting point of NLE theory is the Kuhn segment CM scalar displacement dependent dynamic free energy, $F_{\mathrm{dyn,K}}(r_K)$ (inset of Fig.3b in the main text). At the high packing fractions of interest, the dynamic free energy has a localized form, characterized by a minimum and a local cage barrier, $F_{\mathrm{B,K}}$. Per the ECNLE theory generalization [3,4,7], in the deeply supercooled regime, to achieve a sufficiently large particle hop particles or sites outside the first-shell cage must elastically displace in a collective and correlated manner by a small amount, corresponding to an elastic barrier $\beta F_{\mathrm{B,K}} \approx 2\pi r_{\mathrm{cage,K}}^3 \Delta r_{\mathrm{eff,K}}^2 \rho_{\mathrm{K}} K_{0,\mathrm{K}}$. The mean activated barrier hopping time is computed as the mean first passage time from Kramers theory [19, 20]

$$\tau_{\mathrm{hop,K}} = \frac{2\tau_{\mathrm{s,K}} e^{\beta F_{\mathrm{el,K}}}}{\sigma_{\mathrm{K}}^2} \int_{r_{\mathrm{loc,K}}}^{r_{\mathrm{loc,K}}+\Delta r_{\mathrm{K}}} dr_{\mathrm{K}} e^{\beta F_{\mathrm{dyn,K}}(r_{\mathrm{K}})} \int_{r_{\mathrm{loc,K}}}^{r_{\mathrm{K}}} dr'_{\mathrm{K}} e^{-\beta F_{\mathrm{dyn,K}}(r'_{\mathrm{K}})} \tag{4}$$

where $\tau_{\mathrm{s,K}} = \sigma_{\mathrm{K}}^2 / D_{\mathrm{s,K}}$ (with $\sigma_{\mathrm{K}} = N_{\mathrm{K}}^{1/3}\sigma$) is the characteristic fast process relaxation time for a Kuhn unit and the well-known formula for $D_{\mathrm{s,K}}$ is given elsewhere [3, 7].

B. Mapping idea

The well-developed approach to map theoretical calculations for hard chains to the analogous chemically specific melts in temperature space at 1 atm is adopted here [21-23]. For the PnBA melt or network studied, the experimental Kuhn length [3, 24] is $l_{\mathrm{K}} = 1.72\mathrm{nm}$, and in the tangent Koyama SFC model $\frac{l_{\mathrm{K}}}{\sigma} = \frac{2\xi_{\mathrm{p}}}{\sigma} - 1$. This yields $\sigma = 1.03\mathrm{nm}$ based on using $\xi_{\mathrm{p}}/\sigma = 4/3$ per the discussion in Section II-A and elsewhere [2, 3]. In the mapping approach [21-23] the dimensionless compressibility, $S_0(\phi_{\mathrm{eff}})$, computed from PRISM theory for the Koyama SFC model [13, 14] is equated to $S_0(T)$ obtained from experimental equation of state (EOS) data [24, 25] for PnBA melts. The latter was only measured in the high and medium supercooled regime [24, 25] (over the range T_g/T=0.46-0.74) and thus we employ an analytic representation derived from the

van der Waals model [26], $S_0^{-1} = N_s(B'/T - A')^2$ to model the experimental EOS data [24, 25]. We previously verified that reasonable variation of N_s does not affect our analysis since the crucial aspect is the *T*-dependence of S_0 that is determined by the EOS parameters $A' = 0.5271$ and $B' = 1141.53\text{K}$, and N_s enters only as a *T-independent* prefactor [21, 26, 27]. The final step of our model construction is to set $N_s = 6.51$ to reproduce the experimental glass transition temperature of T_g = 226K of pure PnBA melts [3, 28].

C. SCCH theory for shaped penetrants.

The derivative of the penetrant dynamic free energy in polymer melts based on SCCH theory [2, 8-10] is formulated at a CM level where the total force on the molecule involves polymer-induced forces on all sites of the penetrant. This is the only new aspect, and the effective force on the penetrant at the dynamic free energy level is straightforwardly given by:

$$\frac{\partial \beta F_{\text{dyn,p}}(r_p, r_K)}{\partial r_p} = -\frac{3}{r_p} + \frac{N_p r_p}{3}\int \frac{d\mathbf{q}}{(2\pi)^3} q^2 \rho \omega_p(q) C_{mp}^2(q) S_{mm}(q) e^{-q^2 r_p^2/6} e^{-q^2 r_K^2 \omega_K(q)/6 S_{mm}(q)} \quad (5)$$

Adopting the neutral pinning model of crosslinked polymer networks [3, 8], Eq.(5) is modified as:

$$\frac{\partial \beta F_{\text{dyn,p}}(r_p, r_{Ku})}{\partial r_p} = -\frac{3}{r_p} + \frac{N_p r_p}{3}\int \frac{d\mathbf{q}}{(2\pi)^3} q^2 \omega_p C_{mp}^2(q) e^{-q^2 r_p^2/6}$$

$$\times [S_{uu}(q, r_{Ku}) + S_{nn}(q, r_{Ku}) + S_{un}(q, r_{Ku}) + S_{nu}(q, r_{Ku})] \quad (6)$$

Here, the subscript notation Ku and Kn refer to the mobile (unpinned) Kuhn segments and immobile (pinned) sites, respectively, and the $S_{\alpha\theta}(q, r_{Ku})$ in Eq.(6) are the collective partial Debye-Waller factors of the polymer matrix, which differ from a melt of fully mobile segments, as previously derived [3, 29]. When $N_p = 1$ and hence $\omega_p(q) \equiv 1$, Eqs.(5) and (6) simplify to the original form of the dynamic free energy for hard sphere penetrants [2, 8].

To render SCCH theory predictive and tractable, the degree of Kuhn segment dynamic displacement that facilitates penetrant hopping is described by introducing a trajectory coupling variable, γ, defined as [2, 8-10]: $r_{\mathrm{Ku}}(\gamma) - r_{\mathrm{loc,Ku}} = (r_{\mathrm{p}} - r_{\mathrm{loc,p}})/\gamma$. This parameter is determined based on enforcing a *temporal self-consistency* condition [2, 8-10]: $\tau_{\mathrm{hop,p}}(\gamma) = \tau_{\mathrm{dis,K}}(\Delta r_{\mathrm{Ku,c}}(\gamma))$, where $\Delta r_{\mathrm{Ku}}(\gamma) = \Delta r_{\mathrm{p}}(\gamma)/\gamma$ and $\tau_{\mathrm{hop,p}}(\gamma)$ and $\tau_{\mathrm{dis,K}}(\Delta r_{\mathrm{Ku,c}}(\gamma))$ are computed using Kramers theory as sketched in Eq.(4) but using the penetrant dynamic free energy and Kuhn segment dynamic free energy, respectively. Solving the self-consistency condition yields γ which depends on all system control parameters. In computing $\tau_{\mathrm{hop,p}}$ and hence $\tau_{\alpha,\mathrm{p}}$, the prefactor $\tau_{\mathrm{s,p}} = d_{\mathrm{eff}}^2/D_{\mathrm{s,p}}$ is a characteristic short-time scale for penetrants which is assumed to be determined by penetrant effective total diameter d_{eff} and $D_{\mathrm{s,p}}$, thereby yielding the N_{p}-dependent $D_{\mathrm{s,p}}$,[9, 10]

$$
\begin{aligned}
D_{\mathrm{s,p}} &= \frac{D_{\mathrm{E,p}}}{N_{\mathrm{p}}}\left[1+\frac{1}{6\pi^2}\int_0^\infty dq q^2\,\frac{\rho C_{\mathrm{mp}}^2(q)S_{\mathrm{mm}}(q)}{1+\left(D_{\mathrm{E,m}}/D_{\mathrm{E,p}}\right)n(q)/S_{\mathrm{mm}}(q)}\right]^{-1} \\
D_{\mathrm{E,p}} &= \frac{\sigma^4}{\tau_0 d_{\mathrm{mp}}^2}\left(\frac{m+M}{2m}\right)^{1/2} g_{\mathrm{mp}}^{-1}(d_{\mathrm{mp}})
\end{aligned}
\tag{7}
$$

where m and M are the penetrant and matrix (polymer monomer) site masses, respectively, $m/(m+M) = d_{\mathrm{s}}^3/(d_{\mathrm{s}}^3 + \sigma^3)$, and $1/n(q)=1-j_0(q)+2j_2(q)$ with $j_\alpha(q)$ the Bessel function of order α.

A collective elastic fluctuation of the polymer matrix, and hence an elastic barrier, is required to allow the penetrant to hop.[3, 6, 7] This physics enters via *a common* elastic barrier ($F_{\mathrm{el,p}} = F_{\mathrm{el,Ku,c}}$) in the computation of the timescale $\tau_{\mathrm{hop,p}}(\gamma) = \tau_{\mathrm{dis,K}}(\Delta r_{\mathrm{Ku,c}}(\gamma))$. The elastic barrier has been derived as $\beta F_{\mathrm{el,p}} \approx 2\pi(1-f_{\mathrm{n}})r_{\mathrm{cage,p}}^3 \Delta r_{\mathrm{eff,p}}^2 \rho_{\mathrm{K}} K_{0,\mathrm{K}}$ where $\Delta r_{\mathrm{eff,p}}(\gamma) \approx 3\Delta r_{\mathrm{Ku,c}}^2/32 r_{\mathrm{cage,p}}$, $r_{\mathrm{cage,p}} = r_{\mathrm{min,mp}}(d + N_{\mathrm{K}}^{1/3}\sigma)/(d+\sigma)$, and $r_{\mathrm{min,mp}}$ is the cage radius corresponding to the first minimum of cross radial distribution function $g_{\mathrm{mp}}(r)$.[2, 8]

When considering penetrant shape effects, the Kuhn segment localized state spring constant $K_{0,\mathrm{K}}$ is identical to its pure polymer system value in the *dilute* penetrant limit of interest. Thus, the penetrant shape dependence of its elastic barrier arises entirely to the cooperative Kuhn segment facilitated displacement $\Delta r_{\mathrm{Ku,c}}$. As shown in plots below, $\Delta r_{\mathrm{Ku,c}}$ increases significantly with the degree of penetrant shape asymmetry or N_{p}, which provides the underlying reason for why in Figs.9d, 9e, and 9f a significant shape dependence of elastic barrier is predicted.

III. Additional Results

A. Penetrant alpha time scales

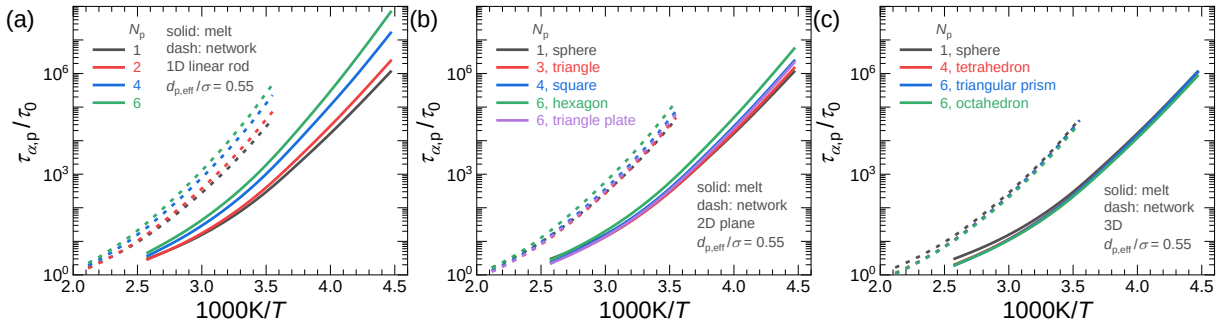

Fig.S1. Same displays as Fig.10 for the penetrant alpha relaxation time for penetrants of different shapes, $\tau_{\alpha,\mathrm{p}}/\tau_0$, with $d_{\mathrm{eff}}/\sigma = 0.55$ in both a polymer melt (solid) and heavily crosslinked network (dash), but now plotted versus $1000\mathrm{K}/T$, for (a) 1D, (b) 2D, and (c) 3D like penetrants.

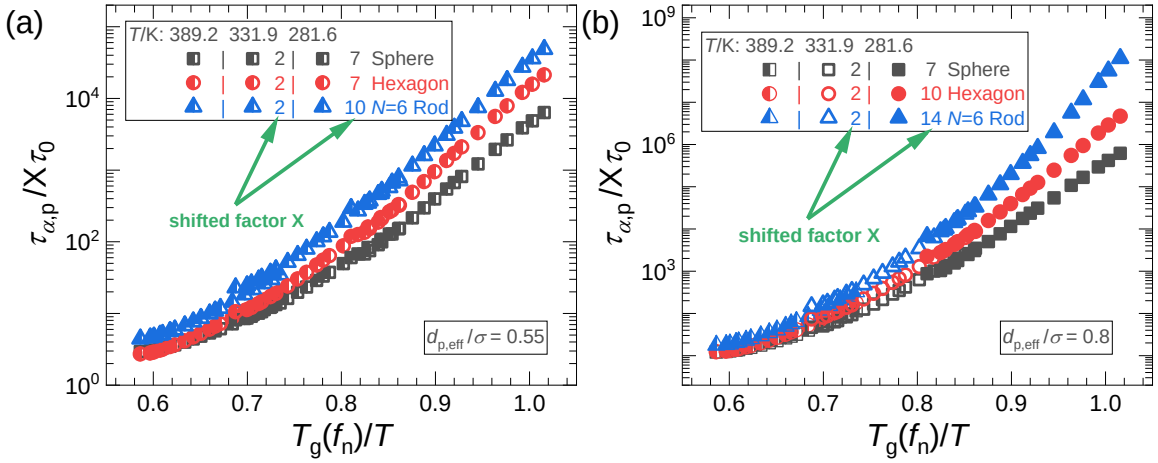

Fig.S2. Same displays as in Fig.11: penetrant mean alpha time as a function of $T_g(f_n)/T$ at various fixed temperatures and three penetrant shapes (sphere, hexagon, and $N_p = 6$ rod) for d_{eff}/σ equaling (a) 0.55 and (b) 0.8, respectively, but now with the y-axis value at the two lower temperatures shifted down to achieve a master curve by a factor of "X" as listed in the legends.

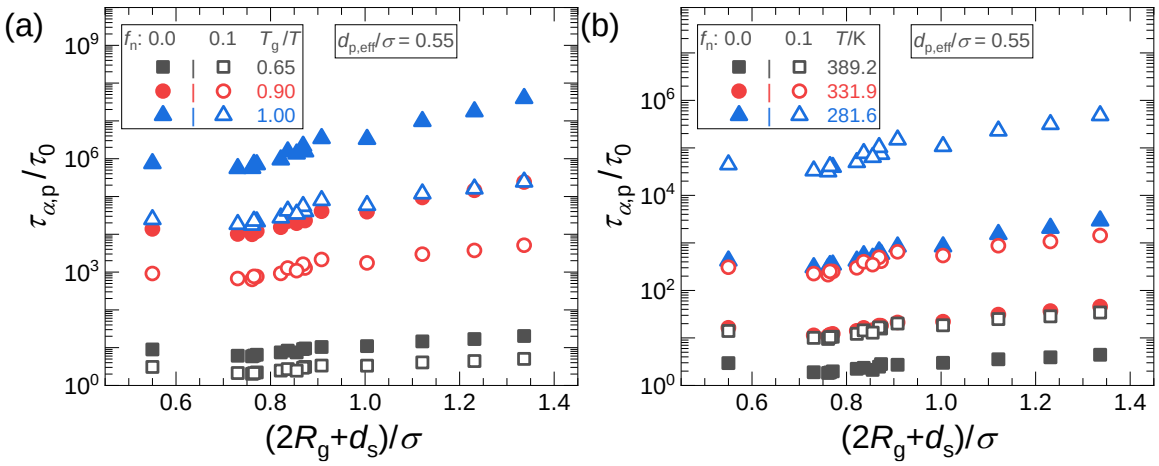

Fig.S3. Same displays as in Fig.12 for the penetrant alpha time as a function of the aspect ratio variable at (a) fixed T_g/T and (b) fixed inverse temperature in a polymer melt (solid) and heavily-crosslinked network (open) over a wide range of penetrant shapes and temperatures, but now for the smaller penetrant size d_{eff}/σ =0.55. From the left to right, the penetrant shapes are sphere, octahedron, triangular dipyramid, triangular prism, tetrahedron, triangle, square, triangle plate, pentagon, rod in $N_p = 2$, hexagon, rod in $N_p = 3$, rod in $N_p = 4$, rod in $N_p = 5$, and rod in $N_p = 6$.

B. Penetrant-to-polymer alpha time ratio

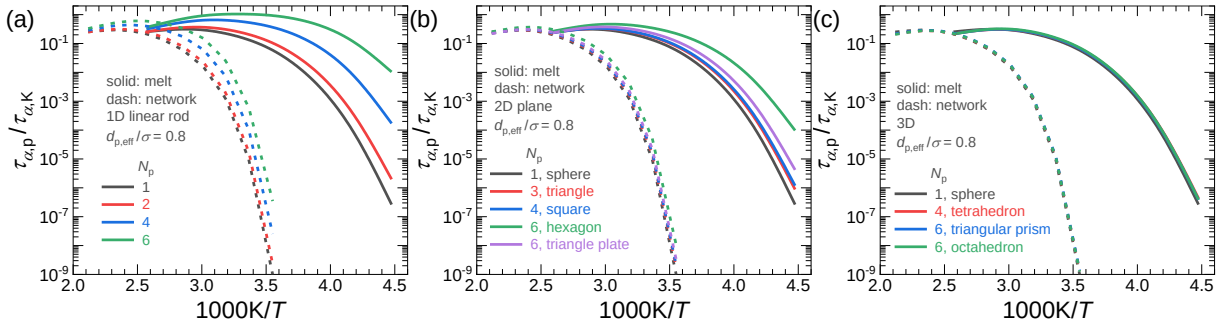

Fig.S4. Same displays as in Fig.13 for the degree of alpha time decoupling between penetrant and Kuhn segment dynamics as quantified by the ratio $\tau_{\alpha,\mathrm{p}}/\tau_{\alpha,\mathrm{K}}$ for $d_{\mathrm{eff}}/\sigma = 0.8$ in both polymer melt (solid) and heavily crosslinked network (dash) for various values of 1D (a), 2D (b) and 3D (c) penetrant shapes, but now plotted as a function of $1000\mathrm{K}/T$.

C. Jump distance and decoupling parameters $r_{\mathrm{K}} - r_{\mathrm{K,c}}$ and γ.

The penetrant jump distance Δr_{p} in units of σ is shown in Fig.S5a as a function of T_{g}/T for $d_{\mathrm{eff}}/\sigma = 0.8$. As discussed in section II of the main text, $N_{\mathrm{p}} g_{\mathrm{mp}}(d_{\mathrm{mp}})$ increases as N_{p} grows, and hence the penetrant jump distance decreases with N_{p}. Relative to Δr_{p}, the cooperative displacement of Kuhn segments (relative to its localization length) at penetrant alpha time scale $\Delta r_{\mathrm{K,c}}$ increases with N_{p}, as shown in Fig.S5b. The Kuhn segment displacement (relative to its localization length) at the Kuhn segment alpha time scale Δr_{K} (pink data) is also shown in Fig.S5b. With increasing aspect ratio, it gradually approaches Δr_{K}, suggesting the penetrant-matrix dynamic coupling grows as the penetrant aspect ratio increases, an intuitive trend. For the $N_{\mathrm{p}} = 6$ rod, $\Delta r_{\mathrm{K,c}}$ is slightly larger than Δr_{K}, implying a slaved behavior of penetrant and matrix.

Relative to polymer melts, the penetrant in crosslinked networks needs to displace a larger distance before escaping its cage, and hence the penetrant jump distance Δr_{p} in crosslinked networks is higher than in polymer melts (see Fig.S5a). Given this, and that the trajectory coupling parameter γ does not change much with degree of crosslinking at fixed temperature or T_{g}/T (see

Fig.15b and Figs.S7-S9), one might expect the Kuhn segment facilitation displacement $\Delta r_{\mathrm{K,c}} = \Delta r_{\mathrm{p}}/\gamma$ in networks would be higher than in polymer melts. This expectation is confirmed in Fig.S5b. Given the larger value of $\Delta r_{\mathrm{K,c}}$ for crosslinked networks, one might then expect that the penetrant elastic barrier in networks will be larger for the same range of T_{g}/T since as discussed above the elastic barrier is determined by $\Delta r_{\mathrm{K,c}}$. However, this argument is not correct because in order to fairly compare crosslinked networks with polymer melts, the influence from the polymer Kuhn segment localization spring constant (effective quantifies polymer matrix high frequency elastic modulus) $K_{0,\mathrm{K}}$ must be taken into account, and doing so results in an increase of the degree of decoupling at fixed T_{g}/T. We do find (see Fig.15a) that $\Delta r_{\mathrm{K}} - \Delta r_{\mathrm{K,c}}$ for crosslinked networks is higher than in polymer melts. Hence, the degree of dynamic coupling in networks is smaller than in melts, thereby resulting in a lower elastic barrier for the networks over the same range of T_{g}/T.

All the above trends and predictions remain the same in T_{g}/T and $1000\mathrm{K}/T$ spaces (the latter results are in Fig.S6) except that in $1000\mathrm{K}/T$ space, $K_{0,\mathrm{K}}$ for networks is much higher than in polymer melts at a fixed temperature. Thus, the elastic barrier in melts is much less than that in networks at any fixed temperature. In reduced inverse temperature space, $K_{0,\mathrm{K}}$ at a fixed T_{g}/T in melts corresponds to a much lower temperature, and hence $K_{0,\mathrm{K}}$ is larger than in networks.

Additionally, consistent with our findings for the decoupling time ratio $\tau_{\alpha,\mathrm{p}}/\tau_{\alpha,\mathrm{K}}$, we find from our calculations of $\Delta r_{\mathrm{K}} - \Delta r_{\mathrm{K,c}}$ that the degree of penetrant-polymer coupling in networks is smaller than that in melts for the same range of T_{g}/T. In $1000\mathrm{K}/T$ space, $\Delta r_{\mathrm{K}} - \Delta r_{\mathrm{K,c}}$ cannot fully capture the crosslink effects on penetrant dynamics because the localization spring constants of melts and networks are significantly different. Instead, the time ratio $\tau_{\alpha,\mathrm{p}}/\tau_{\alpha,\mathrm{K}}$ encodes all effects

from crosslinking on penetrant relaxation, and we find the relatively smaller degree of coupling in networks is also true in $1000\mathrm{K}/T$ space over the same range of temperatures (see Fig.S4).

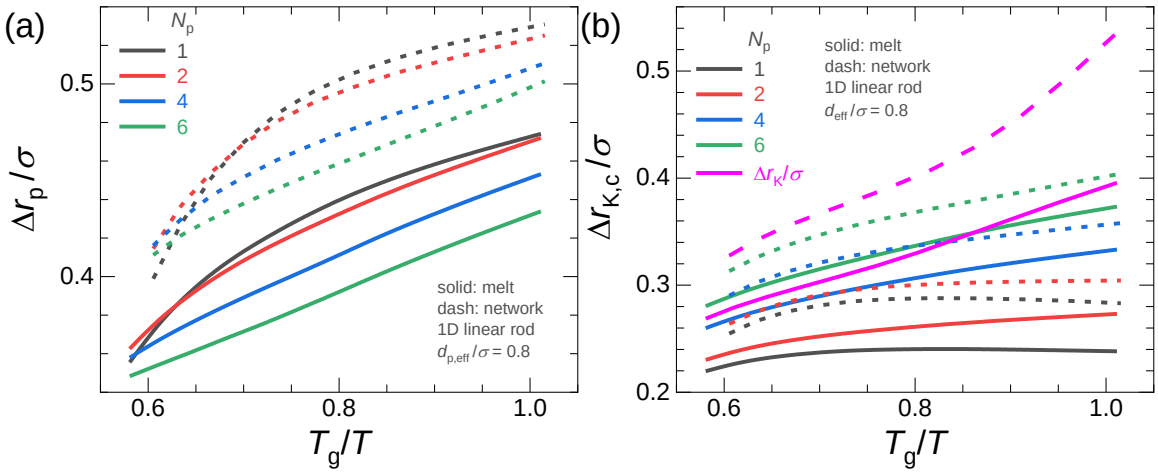

Fig.S5. (a) Penetrant dynamic jump distance Δr_{p} and (b) the facilitation displacement of Kuhn segments (relative to its localization length) at the penetrant alpha time scale $\Delta r_{\mathrm{K,c}}$, as a function of T_{g}/T for $d_{\mathrm{eff}}/\sigma = 0.8$ in polymer melt (solid) and a heavily crosslinked network (dash) over a wide range of 1D-like penetrant shapes. In (b), the Kuhn segment jump distance Δr_{K} (pink curves) is also shown.

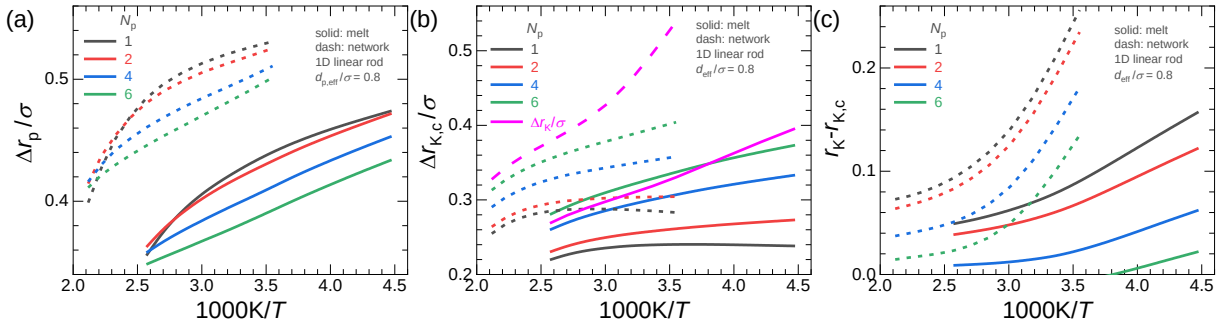

Fig.S6. Same displays as in Fig.S5 for (a) penetrant dynamic jump distance Δr_{p}, and (b) facilitation displacement of Kuhn segments (relative to its localization length) at penetrant alpha time scale $\Delta r_{\mathrm{K,c}}$ for $d_{\mathrm{eff}}/\sigma = 0.8$ in a melt (solid) and network (dash) over a wide range of 1D penetrant shapes, but here now plotted as a function of $1000\mathrm{K}/T$. In (b), the Kuhn segment jump distance Δr_{K} (pink curves) is also shown. (c) Same display as in (a) or (b), but replacing the y-axis with the

displacement difference of Kuhn segment at its alpha time scale relative to that at the penetrant alpha time scale, $r_{\mathrm{K}} - r_{\mathrm{K,c}}$.

The variable γ is directly related to the core self-consistent calculation of SCCH theory that quantifies the cooperative nature of penetrant hopping. By construction, the smaller γ is, the larger is the dynamic coupling of activated penetrant and polymer matrix displacements. As discussed in section II-C, γ is determined based on enforcing a *temporal self-consistency* condition [2, 8-10] which involves the local cage barrier. Hence, its variation with temperature, crosslink density, shape of penetrant, and temperature are different from that of $r_{\mathrm{K}} - r_{\mathrm{K,c}}$ or the alpha relaxation time ratio analyzed in the main text and here.

We presented in the main text only the results for rod-like penetrants at $d_{\mathrm{eff}}/\sigma = 0.8$. Analogous results for the 1D penetrants for $d_{\mathrm{eff}}/\sigma = 0.55$ are shown in Fig.S7, and the 2D and 3D like penetrant cases at both $d_{\mathrm{eff}}/\sigma = 0.8$ and 0.55 are presented in Fig.S8. All behave in a similar manner as that of the 1D-like case results at $d_{\mathrm{eff}}/\sigma = 0.8$. The reason that the behavior of γ for $d_{\mathrm{eff}}/\sigma = 0.8$ remains essentially unchanged for the $d_{\mathrm{eff}}/\sigma = 0.55$ systems (see Fig.14b) is because the penetrant elastic barrier plays no role in determining γ. Hence, the predicted behavior for both penetrant sizes should be similar, as confirmed by comparing results in Fig.15b and Fig.S7.

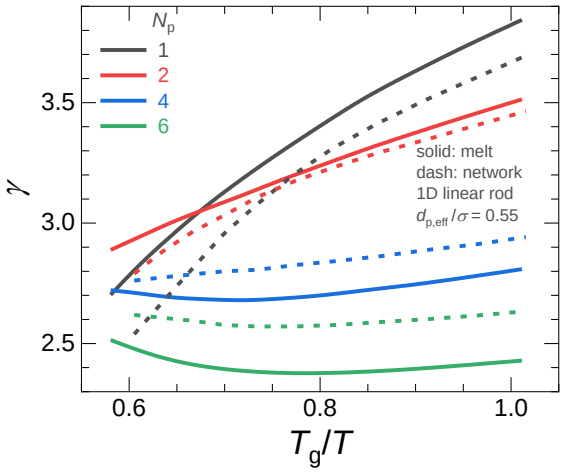

Fig.S7. Dynamic coupling parameter, γ, as a function of T_g/T in a melt (solid) and network (dash) over a wide range of 1D-like penetrant shapes for penetrant size of $d_{\text{eff}}/\sigma = 0.55$.

By comparing the results in polymer melts and crosslinked networks, we find the penetrant shape effects have the same influence on the temperature dependence of their coupling parameter i.e., γ increases with T_g/T at low aspect ratios, but decreases or remains constant at high aspect ratios. However, penetrant shape has a weaker effect on γ in networks (see Fig.15b). Moreover, at low aspect ratios, γ for melts is higher than in networks, while an opposite trend is observed when the penetrant aspect ratio becomes large enough (crossover aspect ratio of ~2) where an identical γ emerges in polymer melts and crosslinked networks over all ranges of T_g/T studied.

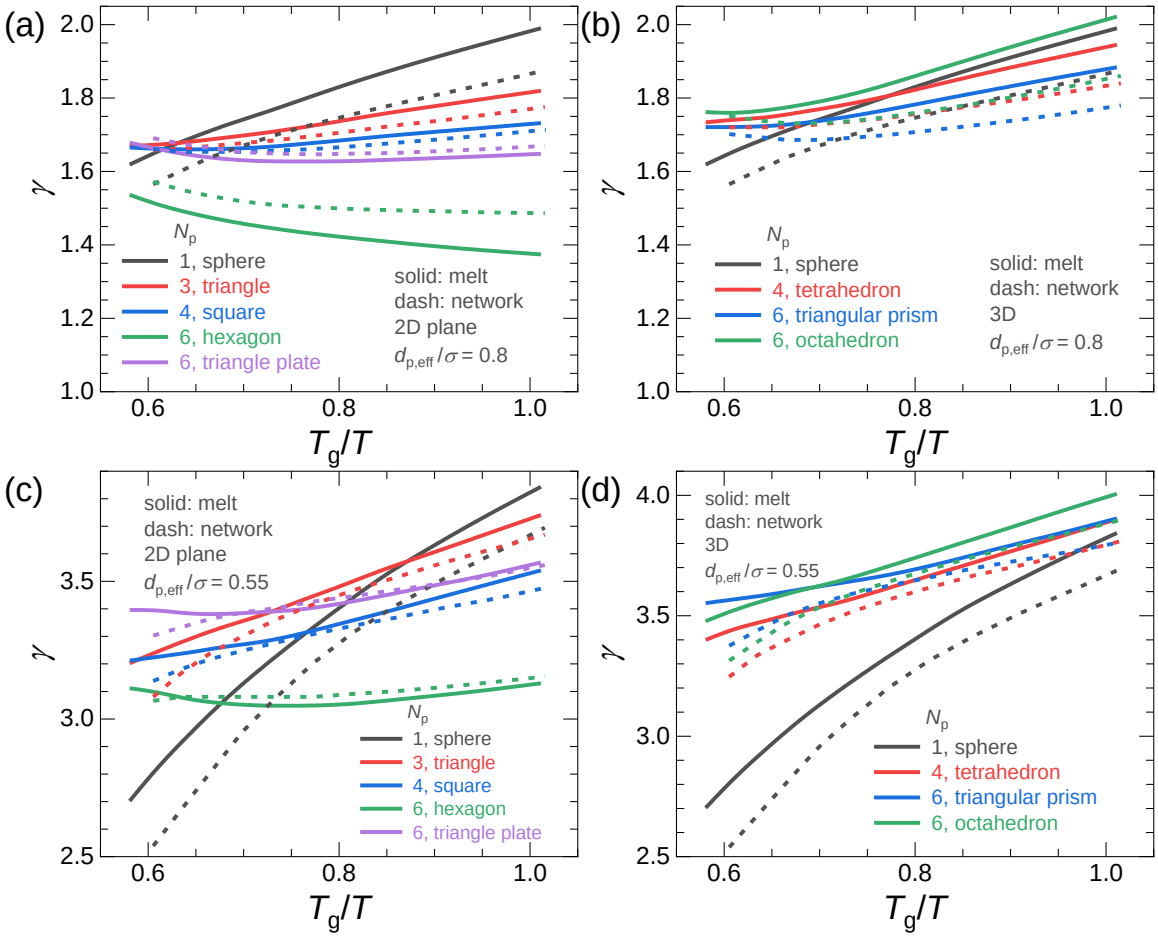

Fig.S8. Same displays as in Fig.14 for the dynamic coupling parameter, γ, in a melt (solid) and network (dash) as a function of T_g/T for penetrant size $d_{eff}/\sigma = 0.8$ (a, b) and 0.55 (c, d), respectively, but now plotted over a wide range of 2D-like (a, c) and 3D-like (b, d) penetrant shapes.

Different from the nonmonotonic dependence of the trajectory coupling parameter predicted in T_g/T space in crosslinked networks and polymer melts, γ in networks in $1000\text{K}/T$ space is always larger than in melts over the same temperature range regardless of the penetrant shape (see Fig.S9). Thus, we deduce that crosslinking contributes more to Kuhn segment dynamics than it affects the penetrant motion, which increases the degree of decoupling (corresponding to a larger γ) between dynamics of Kuhn segment and penetrant.

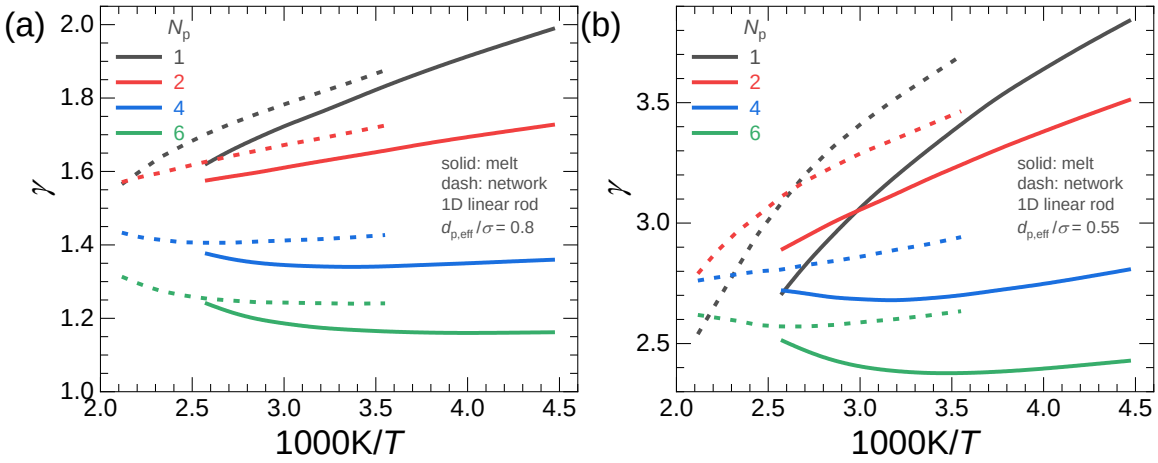

Fig.S9. Same displays as in Fig.15b and Fig.S7 for the dynamic coupling parameter, γ, in a melt (solid) and network (dash) over a wide range of 1D-like penetrant shapes for penetrant size at $d_{\text{eff}}/\sigma = 0.8$ (a) and 0.55 (b), respectively, but now plotted versus $1000\text{K}/T$.

References

1 Y. Zhou, B. Mei and K. S. Schweizer, *J. Chem. Phys.*, 2022, **156**, 114901.

2 B. Mei and K. S. Schweizer, *Macromolecules*, 2022, **55**, 9134.

3 B. Mei, T.-W. Lin, G. S. Sheridan, C. M. Evans, C. E. Sing and K. S. Schweizer, *Macromolecules*, 2022, **55**, 4159−4173.

4 K. S. Schweizer and J. G. Curro, *Adv. Chem. Phys.*, 1997, **1**.

5 K. S. Schweizer and J. G. Curro, *Phys. Rev. Lett.*, 1987, **58**, 246.

6 S. Mirigian and K. S. Schweizer, *J. Chem. Phys.*, 2014, **140**, 194506.

7 B. Mei, Y. Zhou and K. S. Schweizer, *J. Phys. Chem. B*, 2020, **124**, 6121.

8 B. Mei, T.-W. Lin, C. E. Sing and K. S. Schweizer, *J. Chem. Phys.*, 2023, **158**, 184901.

9 B. Mei and K. S. Schweizer, *Soft Matter*, 2021, **17**, 2624.

10 R. Zhang and K. S. Schweizer, *J. Chem. Phys.*, 2017, **146**, 194906.

11 Y. Zhou, B. Mei and K. S. Schweizer, *Phys. Rev. E*, 2020, **101**, 042121.

12 D. Chandler, J. D. Weeks and H. C. Andersen, *Science*, 1983, **220**, 787.

13 K. G. Honnell, J. G. Curro and K. S. Schweizer, *Macromolecules*, 1990, **23**, 3496.

14 R. Koyama, *J. Phys. Soc. Jpn.*, 1973, **34**, 1029.

15 M. Tripathy and K. S. Schweizer, *J. Chem. Phys.*, 2009, **130**, 244907.

16 M. Tripathy and K. S. Schweizer, *J. Chem. Phys.*, 2009, **130**, 244906.

17 G. Yatsenko and K. S. Schweizer, *Phys. Rev. E*, 2007, **76**, 041506.

18 G. Yatsenko and K. S. Schweizer, *J. Chem. Phys.*, 2007, **126**, 014505.

19 H. A. Kramers, *Physica*, 1940, **7**, 284.

20 P. Hänggi, P. Talkner and M. Borkovec, *Rev. Mod. Phys.*, 1990, **62**, 251.

21 B. Mei, Y. Zhou and K. S. Schweizer, *Macromolecules*, 2021, **54**, 10086.

22 S. J. Xie and K. S. Schweizer, *Macromolecules*, 2016, **49**, 9655.

23 S. Mirigian and K. S. Schweizer, *Macromolecules*, 2015, **48**, 1901.

24 B. Mei, G. S. Sheridan, C. M. Evans and K. S. Schweizer, *Proc. Natl. Acad. Sci. USA*, 2022, **119**, e2210094119.

25 D. Walsh and P. Zoller, *Standard pressure volume temperature data for polymers*, CRC press, 1995.

26 B. Mei, Y. Zhou and K. S. Schweizer, *J. Phys. Chem. B*, 2021, **125**, 12353.

27 B. Mei, Y. Zhou and K. S. Schweizer, *Proc. Natl. Acad. Sci. USA*, 2021, **118**, e2025341118.

28 G. S. Sheridan and C. M. Evans, *Macromolecules*, 2021, **54**, 11198.

29 A. Ghosh and K. S. Schweizer, *Macromolecules*, 2020, **53**, 4366.